# Coexistence of ferromagnetism and superconductivity in Sn nanoparticles

W.-H. Li,[*] C.-W. Wang, C.-Y. Li, C. K. Hsu, C. C. Yang, and C.-M. Wu
*Department of Physics, National Central University, Jhongli 32001, Taiwan*
(Received 15 January 2008; revised manuscript received 9 February 2008; published 10 March 2008)

We report on the observations of ferromagnetic spin polarized moment and superconductivity in Sn nanoparticles. Ferromagnetic spin polarization, which is characterized by the appearance of Langevin magnetic-field profiles for magnetization, persists even at room temperature. At temperatures below 15 K, magnetic hysteresis emerges in the weak applied magnetic-field regime. Enhanced superconductivity is found for particles with diameters smaller than 16 nm but larger than 9 nm. The presence of a magnetic field in the superconducting phase reveals a regime in which the magnetic susceptibility and magnetization increase with decreasing temperature. We attribute these behaviors to the coexistence of ferromagnetic spin polarized moment and superconductivity at low temperatures.

## I. INTRODUCTION

Although the microscopic BCS theory for weak coupled superconductivity does not favor the formation of a ferromagnetic superconducting state, the search for ferromagnetic superconductors has continued for several decades. Many magnetic superconductors have been identified. Most of them, however, are associated with antiferromagnetic coupling, where the antiferromagnetic and superconducting electrons are being contributed from chemically well separated ions. A ferromagnetic superconductor has yet to be found. It is known that finite-size effects can lead to unusual superconducting and magnetic behaviors. The suppression of superconductivity by quantum confinement,[1–4] the enhancement of superconductivity by the small size effect,[5,6] the oscillation of the superconducting transition temperature with film thickness,[7] the dependence of superconducting parameters on film topology,[8] and the gigantic enhancement of the critical magnetic field[3,5,9] have all been observed. Permanent giant magnetic moments at the surface layers of oxide and boride thin films,[10,11] ferromagnetic spin polarizations in ultra small Au (Refs. [12–14]) and Ag nanoparticles, and a nonuniform magnetization profile within the nanoparticles[15] have also all been observed. These unconventional magnetic behaviors are currently understood by assuming that ferromagnetic spin correlations, which arise from the spin-orbit coupling[16] and from the spreading of Fermi holes,[17,18] will appear in the surface region of the nanoparticle. One particular feature of nanoparticle superconductivity is the possible occurrence of ferromagnetic spin polarization near the particle surface that coexists with superconductivity at low temperatures. In this paper, we report on the observation of ferromagnetic spin polarization in Sn nanoparticles, which gives rise to reentrantlike temperature profiles for the magnetic susceptibility and magnetization in the superconducting phase that develops below 4.05 K. An applied magnetic field clearly reveals the coexistence of superconductivity and ferromagnetic spin polarization at low temperatures.

## II. SAMPLE CHARACTERIZATION

A series of 11 sets of Sn nanoparticle powders are fabricated employing the gas condensation method. The average particle size can be controlled by proper choice of chamber pressure and evaporation rate. High-purity Sn spheres (99.999% pure, 3 mm in diameter) are evaporated in an Ar atmosphere (0.02 and 2 torr) using an evaporation rate of 0.05 Å/s. A stainless steel plate maintained at the liquid nitrogen temperature is used to collect the evaporated particles. After restoration to room temperature, the nanoparticles, which are only loosely attached to the collector, are stripped off. The samples thus fabricated are in powdered form and consist of macroscopic amounts of individual Sn nanoparticles. X-ray diffraction, atomic force microscopy (AFM), transmission electron microscopy (TEM), and x-ray energy dispersive (EDS) spectrum analysis are used to characterize the powdered samples. All the diffraction patterns can be associated with a tetragonal $\beta$-Sn structure. The diffraction peaks appear to be much broader than the instrumental resolution, reflecting the finite-size effect. A representative x-ray diffraction pattern obtained from the sample fabricated using a chamber pressure of 0.1 torr is shown in Fig. 1, where the solid curve indicates the calculated pattern assuming a Gaussian size distribution with a center at 14 nm and a half-width of 2.8 nm. They agree very well. The mean particle diameters determined from the diffraction profiles for
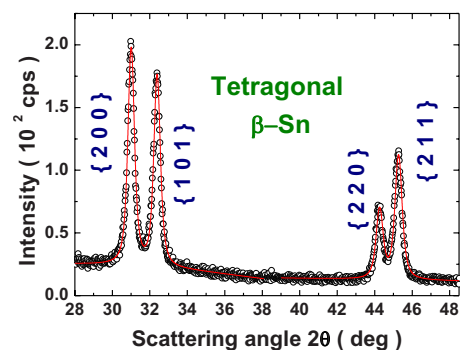


FIG. 1. (Color online) Plot of a portion of the x-ray diffraction pattern of the 14 nm particle assembly revealing a tetragonal $\beta$-Sn structure. Line broadening, resulting from the finite-size effect, can be clearly seen in the diffraction profiles. The solid curves indicate the calculated pattern assuming a Gaussian size distribution with a center at 14 nm and a half-width of 2.8 nm.
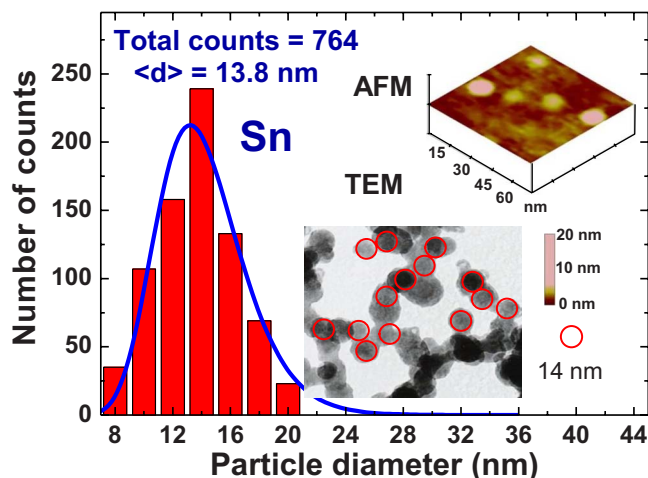
FIG. 2. (Color online) The size distribution of the 14 nm Sn particle assembly obtained from the AFM and TEM images. A symmetrical size distribution is obtained, which may be described by using a Gaussian distribution function (indicated by the solid curve) with a center at 13.8 nm and half-width of 2.8 nm. Portions of the AFM and TEM images are shown as the insets, which indicate that the particles are spherical in nature.

the 11 sets of particles ranged from 3.0(4) to 27(1) nm. Size analyses based on the AFM and TEM images also reveal Gaussian size distributions, with half-widths typically of 1.5 and 3 nm for the particle assemblies with mean diameters smaller and larger than 12 nm, respectively. Portions of the AFM and TEM images obtained on the sample fabricated using a chamber pressure of 0.1 torr and the size distribution obtained from these images are shown in Fig. 2. The solid curve shown in Fig. 2 indicates a Gaussian distribution with a center at 13.8 nm and a half-width of 2.8 nm, obtained from fits of the size distribution data. No noticeable shape asymmetry of the nanoparticles may be identified from the AFM and TEM images. The particles are basically spherical. No SnO diffraction peaks may be identified in all the diffraction patterns, while the EDS analysis indicates that small amounts (<4%) of O are present in the 9, 14, and 20 nm samples.

### III. FERROMAGNETIC SPIN POLARIZATION

The magnetization and ac magnetic susceptibility measurements are performed on a physical property measurement system (PPMS) by Quantum Design employing the standard setups. To avoid the aggregation that may arise among the Sn nanoparticles, the powders are shaken loose at 50 Hz for 5 min using a Vortex–Genie mixer. The powder (~250 mg each) is afterward packed into a thin nonmagnetic cylindrical holder (26 mg, provided by Quantum Design), with a mass density that is ~1.5% that of bulk Sn, which corresponds to an average interparticle separation from edge to edge of 2.7 times the particle diameter. In the temperature regime studied, the holder produces a smooth temperature curve, with signals that is ~0.2% that of the samples.

A Curie–Weiss temperature profile for the in-phase component of the ac magnetic susceptibility $\chi'$ is obtained for
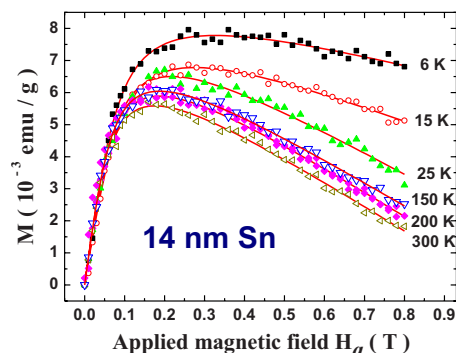


FIG. 3. (Color online) Magnetization curves of 14 nm Sn particles measured in field-increasing loops at several temperatures. The solid curves indicate the fits of the data to a Langevin profile plus a linear diamagnetic response.

temperatures above 4.2 K, revealing a paramagnetic characteristic for the Sn nanoparticles at high temperatures. These $\chi'$ decrease slightly with increasing applied magnetic field $H_a$, reflecting the appearance of diamagnetic responses at high temperatures. Figure 3 shows variations in the magnetization $M$ with the applied magnetic field $H_a$ of the 14 nm particles, taken at several representative temperatures. In the low $H_a$ regime, the magnetization follows a Langevin profile, that is, it increases rapidly with increasing $H_a$, becoming saturated at $H_a \approx 0.3$ T, which signals the existence of ferromagnetic spin correlations. Diamagnetic responses dominate in the high $H_a$ regime, so that the magnetization decreases linearly with increasing $H_a$. When the temperature is reduced to below 15 K, magnetic hysteresis appears in the low $H_a$ regime before $M$ reaches saturation. A representative hysteresis loop taken at 6 K is shown in Fig. 4. Two magnetic components are observed: a paramagnetic component that may be described using the Langevin profile and a diamagnetic one that responds linearly to $H_a$. The solid lines in Fig. 3 show the fitted curves obtained using $M(H_a, T) = M_S(T)L(x) + \chi_D(T)H_a$, where $M_S(T)$ is the saturation magnetization at temperature $T$, $L(x) \equiv \coth(x) - 1/x$ is the Langevin function, $x \equiv \mu_P H_a / k_B T$, $\mu_p$ is the average particle moment, $k_B$ is the Boltzmann constant, and $\chi_D(T)$ is the diamagnetic susceptibility. Good agreements between the observations and the fits are obtained for the measurements made
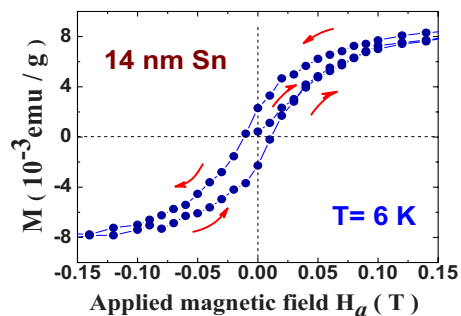


FIG. 4. (Color online) Magnetization loops at 6 K of the 14 nm Sn particles revealing the appearance of magnetic hysteresis in the low field regime.
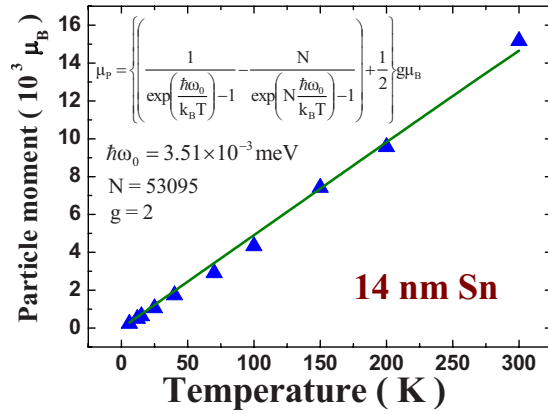
FIG. 5. (Color online) Temperature dependence of the average particle moment of the 14 nm Sn particle assembly showing a linear increase of $\mu_p$ with increasing temperature. The solid line indicates the calculated curve using the expression listed in the inset assuming all the Sn atoms in the 14 nm particles contribute to spin polarization.

at all temperatures. The observed Langevin $M(H_a, T)$ curves may be understood as a randomly oriented assembly of non-interacting ferromagnetic Sn nanoparticles of average particle moment $\mu_p$ at a temperature $T$ that are being aligned by the applied magnetic field $H_a$. In particular, the $M(H_a)$ curves taken at low temperatures follow the Langevin profile nicely, showing that no significant interparticle interaction is present.

The appearance of ferromagnetic spin polarization in nanoparticles is nowadays attributed to the development of uncompensated spins near the particle surfaces,[16–18] originated from the spreading of Fermi holes near the surface and from the transferring of surface charges into the interior of the particles. For 14 nm Sn particles, a spreading of the Fermi holes and/or charges transfer into five layers ($\sim$3 nm) of the interior results in 54% of the atoms contributing to spin polarization, which may be anticipated to be observable. The temperature dependence of $\mu_p$ reveals a linear increase with increasing temperature, as shown in Fig. 5. This unusual behavior of $\mu_p$ increase with increasing temperature has been suggested to be associated with the contributions from thermal excitations of magnons and is known as thermoinduced magnetization.[19] The linear dependence of $\mu_p$ on the temperature agrees with what is expected[20,21] for classical ferromagnetic particles, where the magnetic moment of a particle is taken as from a macrospin. The solid curve shown in Fig. 5 is the calculated $\mu_p(T)$ using the expression listed in the inset, which accounts for the contribution of thermal excitations of the uniform spin-precession modes to the magnetic moment of ferromagnetic nanoparticles.

## IV. ENHANCED SUPERCONDUCTIVITY

Diamagnetic screenings, which result in negative values for $\chi'$, are seen at low temperatures, signaling the occurrence of superconductivity. Figure 6 displays the $\chi'(T)$ of the
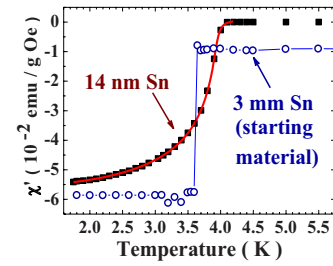


FIG. 6. (Color online) The $\chi'(T)$ curves of the 3 mm and 14 nm Sn particles taken at $H_a$=0 showing that superconductivity of the 14 nm particles develops at a noticeably higher temperature than that of the 3 mm spheres. The solid line on the 14 nm data indicates the fit of the data to the Scalapino expression for superconducting screening.

14 nm particles together with that of the 3 mm spheres (starting material) for a direct comparison. It clearly shows that the diamagnetic screenings of the 14 nm particles begin to develop at a noticeably high temperature than that of the 3 mm spheres. The $\chi'(T)$ of the 14 nm particles may be described very well by the Scalapino expression[22] (solid line). The superconducting transition temperature for the 14 nm Sn particles that we obtained from the fit is $T_C$ =4.05(5) K, which is $\sim$9% higher than that of the 3 mm ones. Superconductivity is observed in all but the 3 and 3.3 nm particle assemblies, for which monotonic increases in $\chi'(T)$ upon cooling to 1.8 K are seen. We note that the critical particle diameter for supporting BCS superconductivity in Sn is 3.24 nm when it is estimated according to the formulas of Anderson[23,24] and Kubo.[25,26] This agrees with the present observations.

The size dependence of $T_C$ obtained from the fits of $\chi'(T)$ to the Scalapino expression is shown in Fig. 7, where enhanced $T_C$ is seen for particles with diameters lying between 16 and 9 nm. An insignificant electron level spacing of 30 $\mu$eV is expected for the 16 nm Sn particles, indicating that the enhanced superconductivity cannot be a direct result of quantum confinement. Rietveld refining the x-ray diffraction patterns show that both of the tetragonal lattice constants increase progressively as the size of the particle is reduced. The increase rate of the axial lattice constant $c$ is about 1.5
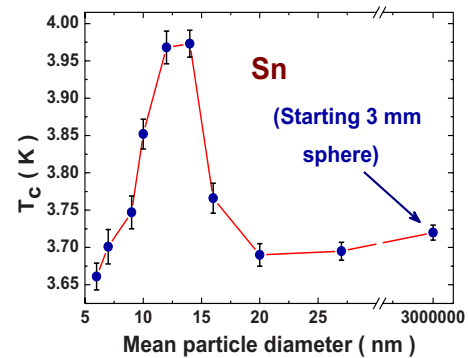


FIG. 7. (Color online) Plot of the variation of $T_C$ with particle diameter revealing an enhanced superconductivity for particles with diameters between 16 and 9 nm.
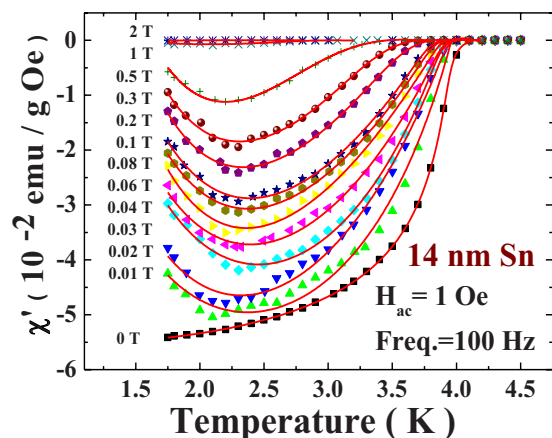
FIG. 8. (Color online) Temperature dependencies of $\chi'$ measured at several $H_a$ employing a probing ac field with a rms strength of 1 Oe and a frequency of 100 Hz. Upturns appear at low temperatures in the measurements made with an $H_a$. The solid curves indicate the fits of the data to a Scalapino term for superconducting screening plus a Curie $C/T$ term for paramagnetic moments.

times that of the basal one, $a$, so that $c/a$ is noticeably altered. Possibly, the enhanced superconductivity is associated with the changes in the $c/a$ ratio. Lattice relaxation and enlarged $c/a$ ratio may cause phonon softening[27,28] and/or an increase in the electronic density of states,[29] which in turn gives rise to an enhanced superconductivity. A similar enhancement regime has also been observed in tetragonal In nanoparticles[5] but not in the cubic Pb nanoparticles.[3]

## V. COEXISTENCE OF SUPERCONDUCTIVITY AND FERROMAGNETISM

Figure 8 shows the variations of $\chi'(T)$ with $H_a$ of the 14 nm particles. Interestingly, an upturn in $\chi'(T)$ appears below $\sim 2.3$ K for the measurement made with an $H_a$. The upturn becomes steeper when a stronger $H_a$ is used. Similar behaviors are also evident in the temperature dependence of the magnetization M(T), as shown in Fig. 9. These $M(T)$ and $\chi'(T)$ curves reveal the existence of a magnetic component
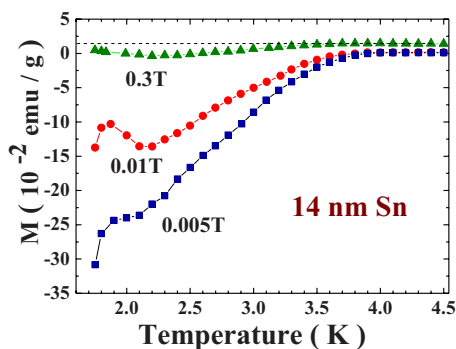


FIG. 9. (Color online) Temperature dependencies of the magnetization measured at several $H_a$. Upturns in $M$ at around 2.3 K are clearly seen. Downturns in $M$ appear at lower temperatures, signaling that superconductivity remains at sufficiently low temperatures.
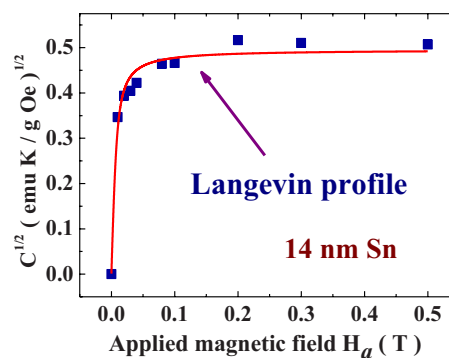


FIG. 10. (Color online) The variations of the square root of the Curie constant with $H_a$, where the solid curve indicates the fit of the data to a Langevin profile.

below $T_C$ and that superconductivity remains at sufficiently low temperatures. The upturn in $\chi'(T)$ may be described using a Curie $T^{-1}$ profile, as expected for the paramagnetic moments observed at high temperatures. The solid lines in Fig. 8 indicate the fitted curves of the observed $\chi'(T)$ to a Scalapino term for superconducting screening plus a Curie $C/T$ term for paramagnetic moments, where the Curie constant $C$ is proportional to $\mu_p^2$. They agree very well. In Fig. 10, we display the variations of $C^{1/2}$ with $H_a$. It reveals an $H_a$ dependence that is very similar to what is observed in the normal state for the ferromagnetic spin polarized moment (illustrated in Fig. 3). In particular, both the $C^{1/2}(H_a)$ curve observed in the superconducting state and the $M(H_a)$ curves observed in the normal state follow the Langevin profile and become saturated at $H_a \approx 0.3$ T, showing that they are associated with the same component. Apparently, superconductivity and ferromagnetic spin polarized moment coexist at low temperatures.

Two components that respond differently to $H_a$ are also evident in the calorimetric data measured below $T_C$. The specific-heat data are collected on a PPMS employing the thermal relaxation method and a charcoal pump placed near the sample platform to avoid He condensation. The nanoparticles are supported using the N-Grease by Apiezon, which produces $\sim 5\%$ of the total signal and a smooth temperature curve. Figure 11 displays the $H_a$ dependence of the thermal variations of the electronic specific heat, where the signals from the N-Grease and the $\beta T^3$ contribution from phonons have been subtracted from the data. Below $T_C = 4.05$ K, two components, marked $\Delta_1$ and $\Delta_2$ in Fig. 11, may be distinguished according to their responses to $H_a$. Clearly, $\Delta_2$ is associated with the occurrence of superconductivity. $\Delta_1$ is strongly suppressed by a relatively weak $H_a$ and becomes relatively insensitive to the field at higher $H_a$. This characteristic $H_a$ dependence of $\Delta_1$ agrees with the entropy that is associated with randomly oriented particle moments being reduced by $H_a$. The $H_a$-independent $\Delta_3$ appears at above $T_C$. The origin of this small component is not completely understood at the present time. It, however, may associate with the emergence of the discrete electron levels anticipated for finite-size particles or relate to the multisize nature of the powder where a distribution of phonon spectrum that cannot be entirely represented by a single $\beta T^3$ curve may be expected.
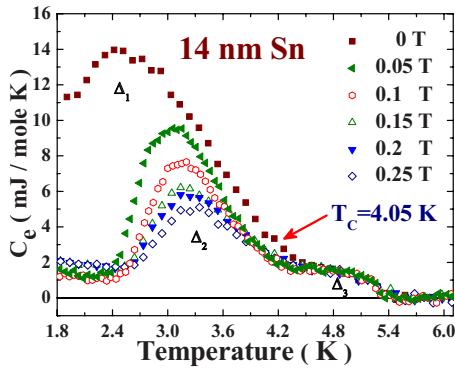
FIG. 11. (Color online) Effects of an applied magnetic field on the thermal variation of the electronic specific heat of 14 nm Sn particles. Three components (marked as $\Delta_1$, $\Delta_2$, and $\Delta_3$) may be distinguished according to their responses to $H_a$. $\Delta_1$ is very sensitive to a weak $H_a$, $\Delta_2$ is associated with the occurrence of superconductivity, whereas the $H_a$-independent $\Delta_3$ appears above $T_C$.

Unconventional cross-shaped $M(H_a)$ hysteresis loops can be found at temperatures below $T_C$. A representative $M(H_a)$ loop taken at 1.75 K is shown in Fig. 12. It departs dramatically from the linear $M(H_a)$ profile expected for type-I Sn. In the field-increasing branches the $M(H_a)$ curves fit nicely (as shown in the inset to Fig. 12) to the Langevin profile, modified by a linear background slope that becomes more pronounced at lower temperatures, resulting from the development of spin polarization moments. A 14 nm particle is far too small to accommodate even a single flux vortex. The type-II-like $M(H_a)$ profile then reflects the characteristic of the penetration of magnetic flux into the particles. It shows that only a portion of the $H_a$ will enter the interior of the particles to be sensed by the superconducting pairs. A substantially higher $H_C$ for nanoparticles than that of their bulk
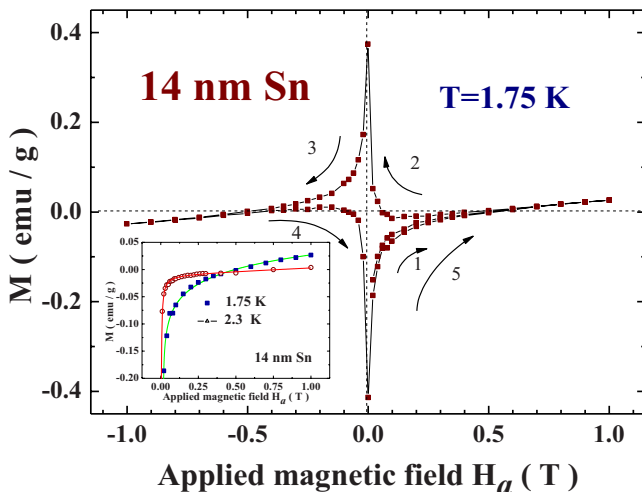


FIG. 12. (Color online) Magnetization loops at 1.75 K of the 14 nm Sn particles revealing an unconventional cross-shaped loop and the appearance of magnetic hysteresis. The inset shows portions of the loops at two representative temperatures, and the solid curves indicate the fits of the data to the Langevin profile plus a linear background slope.
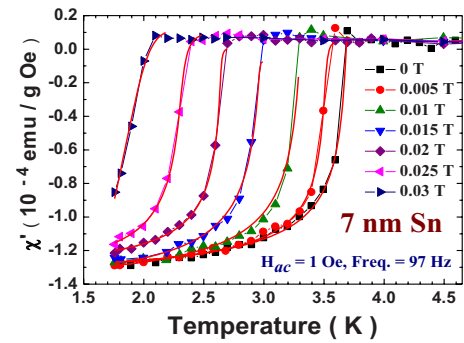


FIG. 13. (Color online) The $\chi'(T)$ curves of the 7 nm particle assembly measured at several $H_a$. The solid curves indicate the fits of the data to the Scalapino expression for superconducting screening.

materials may then be anticipated. Interestingly, the $M(H_a)$ loop displays an asymmetric profile in the field-increasing and field-decreasing branches. Similar $M(H_a)$ loops are obtained at higher temperatures but with the loop width decreasing as the temperature increases. The irreversibility of the entry and exit of magnetic flux lines through the particle surfaces shows that it is mainly the geometric edge barriers[30,31] that control the movements of flux lines at the particle surfaces. This characteristic agrees with the nature of nanoparticles where surface to volume ratio is significant.

The coexistence of superconductivity and ferromagnetism is also observed in the 10, 12, and 16 nm particles, but not in particles larger than 20 nm or smaller than 10 nm (with temperatures reduce to 1.8 K). Figure 13 shows the $\chi'(T)$ curves of the 7 nm particles, measured at various $H_a$. Significantly weaker diamagnetic screenings are seen. They are more than 400 times smaller than that from 14 nm particles. No upturn may be identified in $\chi'(T)$ taken at $H_a \neq 0$ with temperatures reduce to 1.8 K. $T_C$ drops to 3.71 K at $H_a = 0$, and it becomes very sensitive to $H_a$. An $H_a$ of 0.035 T suppresses $T_C$ to below 1.8 K. All these behaviors indicate that the finite-size effect that weakens superconductivity has become important for the 7 nm particles. On the other hand, the ferromagnetic spin polarization of the 7 nm particles further develops. Figure 14 shows the $M(H_a)$ curve of the 7 nm particles taken at 5 K, where the solid line indicates the fit of the data to a Langevin profile plus a linear diamagnetic response. It reveals a saturation magnetization that is 30% higher than that of the 14 nm particles.

## VI. DISCUSSION AND CONCLUSION

The results presented here raise a critical question regarding the origin of the magnetic component that appears in the superconducting phase. Although the EDS spectrum does indicate that 4% of O appears in the 14 nm particles, which corresponds to 22 layers of Sn surrounded by 1 layer of SnO, the ferromagnetism cannot be originated mainly from the outmost SnO layer since the associated moment at $H_a = 0.01$ T is ~30% of the screened moment and the upturn in $\chi'(T)$ is 3 orders of magnitude higher than the SnO may
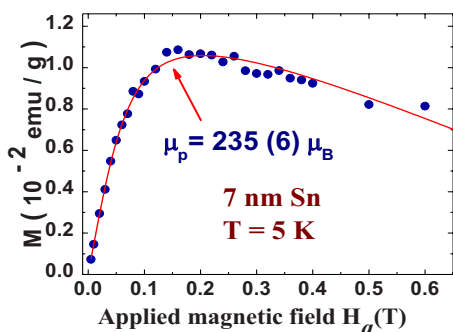
FIG. 14. (Color online) Magnetization curve of the 7 nm Sn particle assembly measured at 5 K. The solid curve indicates the fit of the data to a Langevin profile plus a linear diamagnetic response. An average particle moment of $\mu_p=235(6)\mu_B$ is obtained from the fit.

produce ($10^{-5}$ emu/g Oe at 2 K). Surface enhancement of superconductivity in Sn has been observed.[32] However, surface superconductivity may not be the main mechanism accounting for the present observation since it is difficult to anticipate a 9% increase in $T_C$ from surface enhancement alone and it is difficult to distinguish surface atoms from inner atoms for a 14 nm particle. Enhanced critical magnetic field associated with shape asymmetry has also been observed in Sn.[9] These measurements are performed on relatively large particles and wires, where no enhanced $T_C$ and no ferromagnetism are found. No shape asymmetry is found in the present Sn samples. Shape-dependent superconducting characteristics may then not be revealed in the present study.

It is known that the spin-triplet superconducting component could readily coexist with ferromagnetism.[33] There is, however, no evidence in the present study to support the formation of a spin-triplet state in the extremely space-restricted Sn nanoparticles. One other possible origin for the observed coexistence effect is that the local magnetic field produced by the spin polarized moments is not strong enough to break the enhanced superconducting pairs, so that the spin-singlet superconductivity survives from the local magnetic field. The critical magnetic field $H_C$ of bulk Sn is 309 Oe, showing that the superconducting pairs in bulk Sn can be easily broken by a relatively weak magnetic field. An enhanced superconductivity is then an essential criterion for the superconductivity to survive from the presence of a ferromagnetic moment in extremely space-restricted Sn nanoparticles. It is known that spin polarization becomes insignificant for large particles. The absence of the coexistence effect in large particles is then understandable. Nevertheless, the hiding of the coexistence behavior in smaller particles from this study is not completely understood. Possibly, it may appear at temperatures lower than those achievable in the present study. A strong enough applied magnetic field is needed to reveal a net magnetization from a ferromagnetic particle assembly. For particles having a low $H_C$, such as the 7 nm particles, the alignment field will also suppress $T_C$ to a lower temperature that restricts the observation using this mean. We note that the absences of upturns in $\chi'(T)$ obtained in this study for smaller particles do not necessarily mean that ferromagnetism and superconductivity do not coexist at low temperatures. We believe that the coexistence of ferromagnetic spin polarization and superconductivity may appear in nonmagnetic nanoparticles other than Sn. Ferromagnetic spin polarization must thus be considered in understanding nanoparticle superconductivity.

*Corresponding author: whli@phy.ncu.edu.tw

[1] A. Bezryadin, C. N. Lau, and M. Tinkham, Nature (London) **404**, 971 (2000).

[2] S. Reich, G. Leitus, R. Popovitz-Biro, and M. Schechter, Phys. Rev. Lett. **91**, 147001 (2003).

[3] W.-H. Li, C. C. Yang, F. C. Tsao, and K. C. Lee, Phys. Rev. B **68**, 184507 (2003).

[4] S. Bose, P. Raychaudhuri, R. Banerjee, P. Vasa, and P. Ayyub, Phys. Rev. Lett. **95**, 147003 (2005).

[5] W.-H. Li, C. C. Yang, F. C. Tsao, S. Y. Wu, P. J. Huang, M. K. Chung, and Y. D. Yao, Phys. Rev. B **72**, 214516 (2005).

[6] R. W. Cohen and B. Abeles, Phys. Rev. **168**, 444 (1968).

[7] Y. Guo *et al.*, Science **306**, 1915 (2004).

[8] V. V. Moshchalkov, L. Gielen, C. Strunk, R. Jonckheere, X. Qiu, C. Van Haesendonck, Y. Bruynseraede, Nature (London) **373**, 319 (1995).

[9] Y.-J. Hsu, S.-Y. Lu, and Y.-F. Lin, Small **2**, 268 (2006).

[10] P. O. Lehtinen, A. S. Foster, Y. Ma, A. V. Krasheninnikov, and R. M. Nieminen, Phys. Rev. Lett. **93**, 187202 (2004).

[11] M. Venkatesan, C. B. Fitzgerald, and J. M. D. Coey, Nature (London) **430**, 630 (2004).

[12] Y. Yamamoto, T. Miura, M. Suzuki, N. Kawamura, H. Miyagawa, T. Nakamura, K. Kobayashi, T. Teranishi, and H. Hori, Phys. Rev. Lett. **93**, 116801 (2004).

[13] H. Hori, Y. Yamamoto, T. Iwamoto, T. Miura, T. Teranishi, and M. Miyake, Phys. Rev. B **69**, 174411 (2004).

[14] P. Crespo *et al.*, Phys. Rev. Lett. **93**, 087204 (2004).

[15] G. M. Pastor, J. Dorantes-Dávila, and K. H. Bennemann, Phys. Rev. B **40**, 7642 (1989).

[16] A. Hernando, P. Crespo, and M. A. García, Phys. Rev. Lett. **96**, 057206 (2006).

[17] V. Sahni and K.-P. Bohnen, Phys. Rev. B **29**, 1045 (1984); **31**, 7651 (1985).

[18] M. K. Harbola and V. Sahni, Phys. Rev. B **37**, 745 (1988).

[19] S. Mørup and C. Frandsen, Phys. Rev. Lett. **92**, 217201 (2004).

[20] S. Morup and B. R. Hansen, Phys. Rev. B **72**, 024418 (2005).

[21] S. Mørup, J. Magn. Magn. Mater. **37**, 39 (1983).

[22] B. Mühlschlegel, D. J. Scalapino, and R. Dento, Phys. Rev. B **6**, 1767 (1972).

[23] P. W. Anderson, J. Phys. Chem. Solids **11**, 28 (1959).

[24] J. von Delft, A. D. Zaikin, D. S. Golubev, and W. Tichy, Phys. Rev. Lett. **77**, 3189 (1996).

[25] R. Kubo, J. Phys. Soc. Jpn. **17**, 975 (1962).

[26] See, for example, W. P. Halperin, Rev. Mod. Phys. **58**, 533 (1986).

[27] J. C. Phillips, *Physics of High-$T_C$ Superconductors* (Academic, San Diego, 1989), Chap. 1.

[28] V. L. Ginzburg, Phys. Lett. **13**, 101 (1964).

[29] S. Bose, P. Raychaudhuri, R. Banerjee, P. Vasa, and P. Ayyub, Phys. Rev. Lett. **95**, 147003 (2005).

[30] E. H. Brandt, Phys. Rev. B **59**, 3369 (1999).

[31] M. Pissas, E. Moraitakis, D. Stamopoulos, G. Papavassiliou, V. Psycharis, and S. Koutandos, J. Supercond. **14**, 615 (2001).

[32] V. F. Kozhevnikov, M. J. Van Bael, W. Vinckx, K. Temst, C. Van Haesendonck, and J. O. Indekeu, Phys. Rev. B **72**, 174510 (2005).

[33] S. Keizer, S. T. B. Goennenwein, T. M. Llapwijk, G. Miao, G. Xiao, and A. Gupta, Nature (London) **439**, 825 (2006).